IEEE Robotics and Automation Letters (RA-L) paper, presented at ICRA 2026, Vienna, Austria. Cite as RA-L paper.

# L-BIRD: Lightweight Bio-Inspired Rotary-wing Drone

Xuwen Guo, *Graduate Student Member, IEEE,* Mingxuan Zhu, *Graduate Student Member, IEEE,* and Yinghong Tian, *Member, IEEE*

***Abstract*—In nature, birds exhibit outstanding attitude control, enabling flexible and efficient takeoff, hovering and landing — capabilities that have not been fully replicated. Thus, we introduce the lightweight bio-inspired rotary-wing drone (L-BIRD). It incorporates a spherical structure, which can imitate birds' attitude variation and land on complex surfaces adaptively. L-BIRD employs a model predictive control (MPC) framework to enable real-time tracking of bird-like attitude trajectories derived from bio-inspired parameter pairs. To facilitate lightweight deployment on resource-constrained hardware platforms, we improve MPC framework by multi-path primal-dual neural network (PDNN), matrix sparsity and multiplicative optimization. Experimental results, both in simulations and real-world deployments, demonstrate that L-BIRD realizes accurate and efficient biomimetic attitude control and diverse environmental adaptability. The attitude trajectory mean-square error (MSE) decreases to 0.0042 rad, random access memory (RAM) usage reduces by 39.3%.**

***Index Terms*—Bio-inspired robots, model predictive control (MPC), primal-dual neural network (PDNN), drone control.**

## I. Introduction

FROM perching to hunting, birds exhibit remarkable flight capabilities in nature. They can land and re-takeoff flexibly on various complex surfaces [1], [2], enabled by dynamic adaptation and precise attitude regulation. Although the flight dynamics of a flapping-wing bird differ fundamentally from those of quadcopters, the birds' ability to approach complex surfaces at diverse landing angles and to achieve smooth transitions between multiple flight modes remains worth emulating for quadcopter design. However, how to replicate these flight abilities in bio-inspired research is still a key challenge in the field of bionic flight [3].

Currently, bionic flight research primarily focuses on structural bionics and behavioral bionics. Structural bionics enhance the maneuverability of flying vehicles by imitating the morphological features of bird wings and tails, such as unmanned aerial vehicles (UAVs) with bionic foldable wing design and UAVs with deformable wings [4], [5]. In terms of more advanced behavioral bionics, researchers currently focus on attitude control of flying vehicles [6], [7]. Existing methods usually adopt short-term-horizon control strategies, which focus only on the next control objective [8], [9]. Although these methods can adapt to parameter variations within a certain range, they are difficult to capture the dynamic characteristics in complex environments, and often fail to handle rapid maneuvers which require high agility. To fill this gap, we extract inspiration from bird flight and investigate the mechanisms of attitude adjustment during bird flight. We find that the core of bird flight lies in its flexible attitude adjustment mechanism, which is based on a long-term horizon [10]. This enables birds to respond rapidly to external perturbations in complex environments and send out control signals such as abrupt stop in time. Model predictive control (MPC) has gained widespread adoption owing to its long-horizon predictive capabilities, along with superior performance in handling complex disturbances and input constraints.

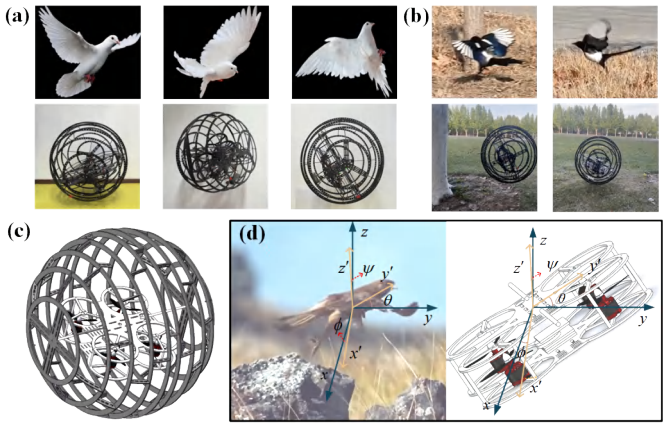


Fig. 1: Design and biomimetic performance of L-BIRD: (a) L-BIRD simulates different flight postures of bird. (b) L-BIRD simulates the landing and re-taking off of birds on complex surfaces. (c) The design of L-BIRD. (d) Comparison of body coordinate system matching between L-BIRD and birds.

However, the high computational complexity and significant hardware memory requirements make it difficult to achieve bird-like real-time attitude control on a low-power, lightweight, and small-memory hardware platform [11], [12]. In addition, birds not only possess the ability to land on various complex surfaces at any time, but also demonstrate the capability to re-takeoff immediately after landing. This flexibility is of vital importance for their hunting, threat avoidance, and environmental exploration [13], [14]. Nevertheless, current research on biomimetic flying vehicles only achieve abrupt stop landings but lack rapid re-takeoff capability [15], [16]. These limitations highlight the need for new structures and control strategies to enhance flight agility and environmental

Xuwen Guo, Mingxuan Zhu and Yinghong Tian are with the Shanghai Key Laboratory of Multidimensional Information Processing, School of Communication & Electronic Engineering, East China Normal University, Shanghai 200241, China (e-mail: 51265904056@stu.ecnu.edu.cn; 51265904076@stu.ecnu.edu.cn; yhtian@cee.ecnu.edu.cn).

**IEEE Robotics and Automation Letters (RA-L) paper, presented at ICRA 2026, Vienna, Austria. Cite as RA-L paper.**

adaptability.

To fill this gap, we have designed the lightweight bio-inspired rotary-wing drone (L-BIRD), a novel biomimetic flying vehicle that integrates both structural and behavioral biomimetic concepts, as illustrated in Fig. 1. L-BIRD employs a spherical outer shell that not only protects the rotors—as in the collision avoidance roll-cage systems of Floreano *et al.* [17], [18], but also enables bird-like landing on complex surfaces and re-takeoff immediately. To better simulate the flight attitude of birds, we propose bio-inspired parameter pairs. This method derives mathematical models of attitude trajectories applicable to medium-sized bird species by fitting photographed bird flight attitudes to idealized model attitude data. Based on this mathematical model, multiple sets of attitude data are generated to iteratively optimize the weight matrices within the MPC framework. This approach enables the system to replicate the dynamic characteristics of bird-like flight across a diverse range of flight attitudes. Additionally, we propose a lightweight optimization that significantly reduces the computational complexity and hardware resource usage. By incorporating sparse matrix structure, multi-path optimization strategies, and sparse algorithm improvements, the system achieves efficient operation on an embedded platform, realizing real-time control of biomimetic attitudes.

## II. Related Work

The ability to land on various surfaces is essential for birds, enabling them to hunt, rest, and observe their surroundings. This capability has inspired the development of biomimetic flying vehicles with versatile landing functionalities, numerous bionic structure designs have been proposed. For instance, studies [15], [16] introduce claw-like mechanisms that enable stable landings by grasping the surface. However, these designs are highly sensitive to the geometry and landing surface, imposing strict constraints on the approach velocity. Similarly, the design in [19] utilizes a surface-gripping mechanism for support, yet it requires a high surface friction coefficient and presents a risk of rotor damage due to its clamping structure. These approaches exhibit notable limitations in adapting to heterogeneous terrains. Consequently, there is a pressing need for novel structural designs and control strategies to enhance the adaptability and robustness of flying vehicles in complex scenarios.

Birds demonstrate remarkable agility in adjusting their attitude within complex natural environments. To emulate this capability, L-BIRD employs an attitude trajectory tracking algorithm designed to maintain dynamic characteristics under varying environmental conditions. In [20], an adaptive sliding mode control (SMC) framework is proposed. However, its effectiveness is strongly dependent on the tuning of controller parameters, and its real-time adaptability in dynamic environments remains limited. Studies [21]–[23] have shown that L1 adaptive control achieves accurate attitude stabilization under disturbances. However, its dependence on a linear reference model and short prediction horizon makes it difficult to fully capture complex and time-varying dynamics, which may lead to suboptimal or unpredictable behavior.

In contrast, MPC has been widely adopted in robotics owing to its long-horizon prediction capability and its effectiveness in preserving dynamic behavior under complex environmental conditions [24], [25]. However, conventional nonlinear MPC (NMPC) typically requires high computational complexity and substantial hardware resource demands, which hinder real-time implementation on embedded platforms. To address these challenges, [26] introduces a linear MPC (LMPC) approach for position control optimization. While this method alleviates computational burden, its linear structure makes it difficult to fully describe the nonlinear attitude dynamics, which in turn restricts its attainable control performance. Alternative optimization strategies have been proposed in [27]; additionally, the Tiny-MPC framework [28] develops an efficient ADMM-based solver aiming at fast, low-memory MPC deployment on microcontrollers. Tiny-MPC still use dense matrix operations, leading to significant computational overhead on highly resource-constrained platforms. Hence, we introduce sparse matrix structure, multi-path optimization strategies, and sparse algorithm improvements to address this problem.

## III. Materials and Methods

### A. L-BIRD System Design

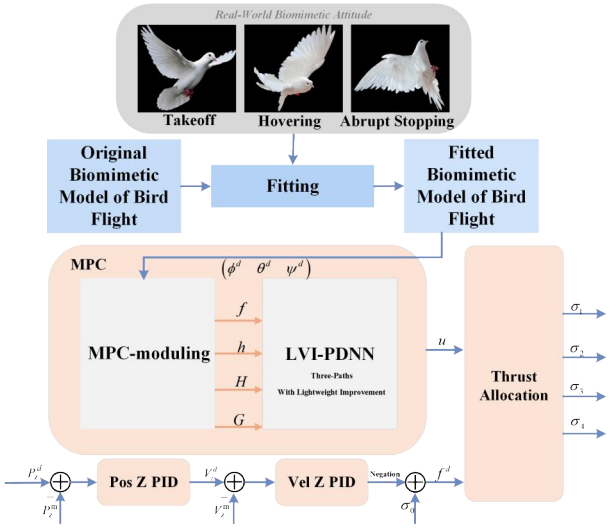


Fig. 2: L-BIRD system block diagram.

By analyzing the ability of birds to stabilize their stay on complex terrains such as branches, slopes, and sand, it can be found that its power system (wings) is separated from the main part of the body during landing or perching. The wings provide flight power, while the main body adjusts its attitude to adapt to the contacting surface. This design allows birds to balance on complex terrain and re-takeoff at any time. Inspired by this, we design a flying vehicle named L-BIRD, aims at simulating the dynamic adaptability and the decoupling of flight power from the main body, as seen in birds. The system block diagram is shown in Fig. 2.

In our design, we place the ”power system” (rotors) inside the structure, while the spherical shell serves as the ”main body”. The outer shell of L-BIRD is made from high-strength

**IEEE Robotics and Automation Letters (RA-L) paper, presented at ICRA 2026, Vienna, Austria. Cite as RA-L paper.**

carbon fiber. The outer shell allows the quadcopter inside to safely operate with a larger range of attitude angles when contacting complex surfaces, as well as to achieve stable perching on any complex surface. A landing-angle sweep test was conducted to verify the MPC-enabled adaptive approach under different surface orientations.

To further enhance system performance, we developed a dynamic model of L-BIRD, which describes its motion characteristics, the distribution of torques, and the attitude adjustment process. The rate of change of the attitude angles can be described by the following equation:

$$\begin{bmatrix} \dot{\phi} \\ \dot{\theta} \\ \dot{\psi} \end{bmatrix} = \begin{bmatrix} 1 & \tan\theta\sin\phi & \tan\theta\cos\phi \\ 0 & \cos\phi & -\sin\phi \\ 0 & \frac{\sin\phi}{\cos\theta} & \frac{\cos\phi}{\cos\theta} \end{bmatrix} \begin{bmatrix} \omega_x \\ \omega_y \\ \omega_z \end{bmatrix}. \quad (1)$$

The control strategy of L-BIRD is based on precise adjustment of angular velocity, enabling flexible attitude control during flight. The rate of change of angular velocity follows the rigid body dynamics equations:

$$\begin{cases} J_{\mathrm{xx}}\dot{\omega}_x = (J_{\mathrm{yy}} - J_{\mathrm{zz}})\omega_y\omega_z + \tau_x, \\ J_{\mathrm{yy}}\dot{\omega}_y = (J_{\mathrm{zz}} - J_{\mathrm{xx}})\omega_z\omega_x + \tau_y, \\ J_{\mathrm{zz}}\dot{\omega}_z = (J_{\mathrm{xx}} - J_{\mathrm{yy}})\omega_x\omega_y + \tau_z. \end{cases} \quad (2)$$

Under small-rate operation, (2) is locally linearized at $\omega \approx 0$, so that the quadratic terms $\omega_i\omega_j$ are neglected as higher-order small quantities, and only the inertia–weighted input influence is retained in (3). By adjusting the rotor thrust distribution, L-BIRD can generate the required control torques flexibly. To simplify the controller design, the above equation can be expressed in terms of an input matrix as follows:

$$\begin{bmatrix} \dot{\omega}_x \\ \dot{\omega}_y \\ \dot{\omega}_z \end{bmatrix} = \begin{bmatrix} \frac{1}{J_{xx}} & 0 & 0 \\ 0 & \frac{1}{J_{yy}} & 0 \\ 0 & 0 & \frac{1}{J_{zz}} \end{bmatrix} \begin{bmatrix} \tau_x \\ \tau_y \\ \tau_z \end{bmatrix}. \quad (3)$$

Related parameters above present in Table I.

TABLE I
NOTATION AND DESCRIPTION

| Notation | Description |
|---|---|
| $\dot{\phi}$ | Change rate of roll angle |
| $\dot{\theta}$ | Change rate of pitch angle |
| $\dot{\psi}$ | Change rate of yaw angle |
| $\omega_x$ | X-axis angular velocity (body coordinate system) |
| $\omega_y$ | Y-axis angular velocity (body coordinate system) |
| $\omega_z$ | Z-axis angular velocity (body coordinate system) |
| $\tau_x$ | X-axis lift and anti-torque moment (world coordinate system) |
| $\tau_y$ | Y-axis lift and anti-torque moment (world coordinate system) |
| $\tau_z$ | Z-axis lift and anti-torque moment (world coordinate system) |
| $J_{xx}$ | X-axis principal moment of inertia (about $1.8 \times 10^{-2}$ kg·m$^2$) |
| $J_{yy}$ | Y-axis principal moment of inertia (about $1.7 \times 10^{-2}$ kg·m$^2$) |
| $J_{zz}$ | Z-axis principal moment of inertia (about $2.5 \times 10^{-2}$ kg·m$^2$) |

Note: In our system, the spherical shell accounts for approximately 40% of the total mass and is evenly distributed, resulting in similar principal moments of inertia.

### *B. Bio-inspired Attitude Trajectory Generation*

The weight of L-BIRD is 862 g, which can simulate the attitude variation process of most medium-sized birds (0.1–1 kg) during different flight phases. Using high-resolution cameras, we recorded video data of various medium-sized birds (e.g., gulls, kestrels, egrets). To extract the attitude information, we employed a keypoint-based pose estimation approach inspired by DeepLabCut [29], with adaptations for L-BIRD's flight. Anatomical landmarks such as the beak, wing tips, and tail were detected across video frames, and their relative positions were mapped into a 3D body coordinate system, that the bird's orientation in pitch, roll, and yaw was reconstructed from monocular video sequences [30]. This process (see Fig. 1(d)) enables a direct comparison between avian and drone attitudes under the same 3D framework.

To enhance the credibility and applicability of the bio-inspired control strategy, we fit the measured bird flight attitude trajectories to equations applicable to a rigid-body model, enabling the generation of attitude trajectories that retain the essential characteristics of bird flight while being suitable for our control framework. The resulting attitude angle variations are derived from the rigid body dynamics equations combined with aerodynamic modeling, describing the attitude characteristics during three key flight phases: takeoff, hovering, and abrupt stop, as shown in Table II.

TABLE II
THE ATTITUDE CHARACTERISTICS DURING THREE FLIGHT PHASES

| Phases | Equation |
|---|---|
| **Takeoff (*TO*)** | $\phi_{TO} = 0$ |
| | $\theta_{TO} = \frac{M_{TO}}{I_y}t - \frac{I_z - I_x}{I_y}(\omega_{z0} + \frac{N_{TO}}{I_z}t)(\omega_{x0} + \frac{L_{TO}}{I_x}t)t$ |
| | $\psi_{TO} = 0$ |
| **Hovering (*HV*)** | $\phi_{HV} = \frac{L_{HV}}{I_x}t - \frac{I_y - I_z}{I_x}(\omega_{y0} + \frac{M_{HV}}{I_y}t)(\omega_{z0} + \frac{N_{HV}}{I_z}t)t$ |
| | $\theta_{HV} = 0$ |
| | $\psi_{HV} = \frac{N_{HV}}{I_z}t - \frac{I_x - I_y}{I_z}(\omega_{x0} + \frac{L_{HV}}{I_x}t)(\omega_{y0} + \frac{M_{HV}}{I_y}t)t$ |
| **Abrupt Stop(*AS*)** | $\phi_{AS} = 0$ |
| | $\theta_{AS} = -\frac{\lvert M_{AS}\rvert}{I_y} + \frac{I_z - I_x}{I_y}(\omega_{z0} + \frac{N_{AS}}{I_z}t)(\omega_{x0} + \frac{L_{AS}}{I_x}t)t$ |
| | $\psi_{AS} = 0$ |

$M_{TO}$ represents the pitch moment during takeoff.
$\omega_z$ and $\omega_x$ represent the angular velocities around the yaw and roll axes, respectively.
$L_{HV}$ represents the roll moment.
$N_{HV}$ represents the yaw moment.
$M_{AS}$ represents the pitch moment during abrupt stop.

To ensure the similarity between the model's attitude angles and the actual measured attitude angles, we input the measured attitude angle data of various medium-sized birds into the attitude angle variation equations for fitting, in order to obtain key parameters. Our paper uses nonlinear least squares fitting, as expressed by the following equation:

$$SSE(p) = \sum_{i=1}^{n} \left(\theta_{\text{measured},i} - f(t_i; p)\right)^2. \quad (4)$$

We compare the matching degree between the measured data and the model's predicted results, ultimately selecting the optimal parameters for subsequent experiments, as shown

**IEEE Robotics and Automation Letters (RA-L) paper, presented at ICRA 2026, Vienna, Austria. Cite as RA-L paper.**

in Table III. We substitute the optimal parameters back into

TABLE III
OPTIMAL CONTROL PARAMETERS

| | **Optimal Control Parameters** |
|---|---|
| $\left(\frac{M_{TO}}{I_y}, \frac{I_z-I_x}{I_y}, \frac{N_{TO}}{I_z}, \frac{L_{TO}}{I_x}\right)$ | (1.461, 1.066, 0.396, 7.133) |
| $\left(\frac{L_{HV}}{I_x}, \frac{I_y-I_z}{I_x}, \frac{M_{HV}}{I_y}, \frac{N_{HV}}{I_z}\right)$ | (0.001, 0.034, 0.048, 0.019) |
| $\left(\frac{N_{HV}}{I_z}, \frac{I_x-I_y}{I_z}, \frac{L_{HV}}{I_x}, \frac{M_{HV}}{I_y}\right)$ | (0.091, 0.004, 0.011, 6.292) |
| $\left(\frac{\lvert M_{AS}\rvert}{I_y}, \frac{I_z-I_x}{I_y}, \frac{N_{AS}}{I_z}, \frac{L_{AS}}{I_x}\right)$ | (49.387, 0.583, 11.265, 3.477) |

the dynamic equations in Table II to generate the time series equations for the attitude angles of L-BIRD. The generated trajectory replicates the bird-like attitude variation characteristics during the takeoff, hovering, and abrupt stop phases.

### *C. Attitude Trajectory Tracking Algorithm*

To achieve precise tracking of L-BIRD's attitude trajectory, this paper employs an MPC-based attitude control algorithm. MPC dynamically adjusts control inputs by performing multi-step predictions and optimizations of future states, in order to minimize the deviation between the system state and the target attitude trajectory. This method is well-suited for L-BIRD's attitude tracking task, as it effectively handles external disturbances and system uncertainties.

In the MPC framework of L-BIRD, state vector $x_k$ is a collection of six state variables $x_k$=[$\phi_k$, $\theta_k$, $\psi_k$, $\omega_{x,k}$, $\omega_{y,k}$, $\omega_{z,k}$]. ngular velocities of the three axes upward, respectively. The control input vector $u_k$ is defined as the moment and thrust inputs in attitude control $u_k$=[$u_1$, $u_2$, $u_3$, $u_4$], where $u_1$ represents the total thrust of L-BIRD, which is derived from force analysis, $u_2$, $u_3$, and $u_4$ represent the moments of the L-BIRD around each axis, respectively. The system's dynamic behavior is represented using a discrete state-space model, with the state transition equation given by:

$$x_{k+1} = \mathbf{A_k} x_k + \mathbf{B} u_k. \tag{5}$$

Where matrix $\mathbf{A_k}$ is a time-varying nonlinear matrix whose elements depend on the current attitude angles, describing how the current state influences the evolution of the attitude and angular velocity. Matrix $\mathbf{B}$ represents how control inputs affect the angular acceleration based on the principal moments of inertia($\mathbf{J_{xx}}$, $\mathbf{J_{yy}}$, $\mathbf{J_{zz}}$). To achieve precise tracking of the target attitude trajectory, a cost function $J$ is constructed to quantify the deviation between the current system state and the target trajectory:

$$J = \sum_{k=0}^{N-1} \|\mathbf{W_y}(y_{k+1} - r_{k+1})\|_2^2 + \|\mathbf{W_u} u_k\|_2^2. \tag{6}$$

Where $y_{k+1}$ is output attitude, and $r_{k+1}$ is the target attitude trajectory, used as the reference input. $\mathbf{W_y}$ and $\mathbf{W_u}$ are the weight matrices for attitude deviation and control input, respectively, and the selection is based on the bio-inspired target attitude trajectory tracking error.

Although our MPC formulation is nonlinear, we perform local linearization at each sampling step, so that the resulting finite-horizon problem can be approximated and solved online as a convex quadratic program (QP), and the optimization problem can be rephrased as follows:

$$\min_z J = \frac{1}{2} z^T \mathbf{H} z + \left(\mathbf{F} x_0 + \overline{\mathbf{S}}^{\mathbf{T}} \overline{\mathbf{K}}^{\mathbf{T}} r\right)^T z \tag{7a}$$

$$s.t. \quad \mathbf{G} z \leq \mathbf{h}. \tag{7b}$$

Where matrices $\mathbf{G}$ and $\mathbf{H}$ are determined by the system's state transition characteristics. Notably, the outer shell effectively relaxes the attitude constraints in the MPC's QP formulation. This expansion of the feasible region improves control robustness. To efficiently solve the QP problem, this paper adopts a primal-dual neural network (PDNN) based on linear variational inequality (LVI) theory [31], [32]. The advantage of it lies in the ability to adapt to inequality constraints and physical boundaries. The solution flowchart of PDNN for each state variable is shown in Fig. 3.

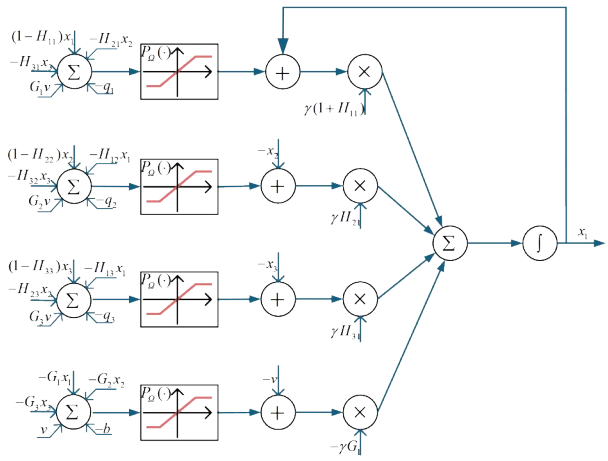

Fig. 3: The solution flowchart of PDNN for each state variable.

Within the PDNN, the optimization problem is transformed into a linear variational inequality, where the goal is to find a vector $\mathbf{y}$ that meets:

$$\begin{cases} (\mathbf{y} - \mathbf{y}^*)^T (\mathbf{H}\mathbf{y}^* + \mathbf{p}) \geq 0, \\ \mathbf{y} = \begin{bmatrix} \mathbf{x} \\ \mathbf{v} \end{bmatrix}, \quad \varsigma^- = \begin{bmatrix} \xi^- \\ 0 \end{bmatrix}, \quad \varsigma^+ = \begin{bmatrix} \xi^+ \\ +\infty \end{bmatrix}. \end{cases} \tag{8}$$

Where $y = [x; v]$ collects the primal and dual variables, $\zeta^-, \zeta^+$ define the feasible box region $\Omega = [\zeta^-, \zeta^+]$, and $\mathbf{H}$, $\mathbf{p}$ are constructed from the KKT conditions of (8) [31].

By the projection under the boundary constraints, we ensure that the updates in each iteration satisfy the constraint conditions, allowing the algorithm to converge stably under the constraints. The projection operator is defined as:

$$P_\Omega(\mathbf{y} - (\mathbf{H}\mathbf{y} + \mathbf{p})) - \mathbf{y} = 0. \tag{9}$$

Therefore, the final update equation for PDNN can be expressed as:

$$\dot{\mathbf{y}} = \gamma \left(\mathbf{I} + \mathbf{H}^{\mathbf{T}}\right) \left(P_\Omega \left(\mathbf{y} - (\mathbf{H}\mathbf{y} + \mathbf{p})\right) - \mathbf{y}\right). \tag{10}$$

Here, $\gamma$ is the step size parameter, which determines the convergence rate of the iteration. Proper selection of the step size parameter allows for improved solving speed while maintaining both the stability and accuracy of the solution.

**IEEE Robotics and Automation Letters (RA-L) paper, presented at ICRA 2026, Vienna, Austria. Cite as RA-L paper.**

### D. Lightweight Improvement

To enable L-BIRD's attitude control algorithm to run in real time on resource-constrained embedded hardware for lightweight flight, it is necessary to improve the computational efficiency of MPC. This paper reduces computational complexity and accelerates processing speed by incorporating sparse matrix structure, multi-path optimization strategies, and sparse algorithm improvements.

As shown in Fig. 4(a), the multi-path optimization strategy proposed in this study assigns each optimization path a distinct initial guess and state configuration. By performing parallel computation of multiple optimization paths and independently solving the dynamic equations along each path, the result of the path that is closer to the objective value is finally selected as the input for the next iteration. The algorithm can choose a larger step size at the beginning of the iteration to quickly approach the vicinity of the target value. Once near the target, a smaller step size can be selected to finetune the results and achieve a more precise output. This approach can significantly accelerate the solving process when dealing with complex, dynamic systems, reduce the number of iterations required to reach convergence, and minimize the consumption of computational resources.

In the solving process, PDNN typically needs to handle large-scale process matrices, which often contain a significant number of zero elements. These zero-value elements do not contribute to the matrix computations. As illustrated in Fig. 4(b), we store only the non-zero elements of the sparse matrix along with their row and column indices, and perform matrix multiplication operations solely on these stored elements. This approach can significantly reduce memory usage and computational burden.

## IV. Experimental Results

### A. Simulation Deployments of Attitude Tracking

To validate the bio-inspired control effectiveness of the L-BIRD control algorithm across different flight stages, we analyze the impact of different weight parameters $\mathbf{W_y}$ and $\mathbf{W_u}$ on attitude tracking performance. Simulation experiments are designed and conducted for three key flight stages: takeoff, hovering, and abrupt stop. The bird flight attitude trajectories obtained from the previous fitting process are used as the target attitude for L-BIRD, and are input into the control algorithm.

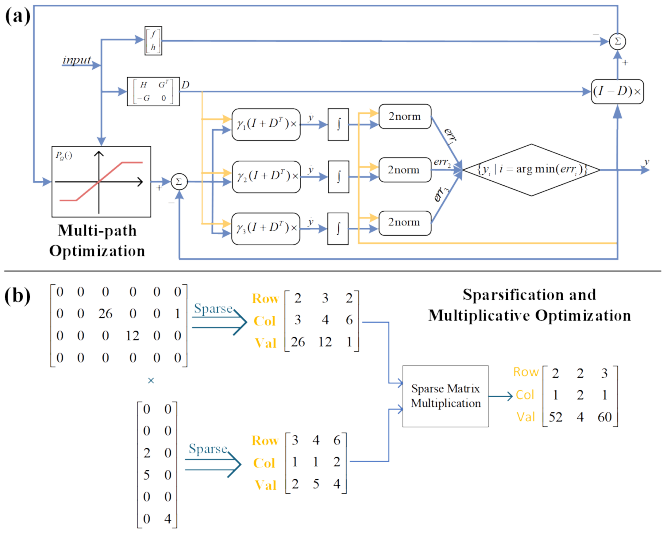


Fig. 4: The lightweight improvements of PDNN.

To obtain the optimal weight parameters $\mathbf{W_y}$ and $\mathbf{W_u}$, we set the traversal range for the main attitude angle weights in $\mathbf{W_y}$ ($\mathbf{W_y} = diag([a, b, c])$. For example, in the takeoff phase, which is mainly a pitch angle change, we fix the weights of the other two attitude angles and change the $\theta$ alone, which is the b in the $\mathbf{W_y}$ equation) to be $[0.5, 1.4]$, with a minimum step size of 0.01. For the main attitude angle weights in $\mathbf{W_u}$ ($\mathbf{W_u} = k \cdot eye(3)$), we set the traversal range to be $[0.5, 5]$, with a minimum step size of 0.05. Based on the previously constructed cost function $J$ and mean-square error (MSE), two sets of experiments are conducted, using $J$ and MSE as the selection criteria for $\mathbf{W_y}$ and $\mathbf{W_u}$. $J$ is the sum of MSE and the control input deviation, focusing on the overall trade-off between the accuracy of the attitude trajectory tracking and the smoothness of the control inputs. On the other hand, MSE specifically emphasizes the degree of alignment between the attitude trajectory and the target trajectory.

We validates the results of selecting the weight parameters in terms of MSE and in terms of $J$ as the heat value in the three typical phases, the selected weight parameters are shown in Fig. 5. From the trajectory plots shown in Fig. 6 and Fig. 7, it can be observed that compared to the trajectory obtained using $J$ as the weight parameter selection criterion, the trajectory generated by selecting the weight matrix parameters based on MSE aligns more closely with the target trajectory.

### B. Lightweight Algorithm Validation

To validate the performance of the lightweight improved MPC algorithm on resource-constrained hardware platforms (XC7Z100), the experiment conducted a detailed analysis from multiple perspectives, including algorithm efficiency, attitude deviation, and memory usage.

We first compare the attitude tracking accuracy of different methods throughout the entire flight phase, as shown in Fig. 8. The results show that the PDNN algorithm with multi-path optimization significantly reduces the attitude deviation. It's worth noting that although the 5-path PDNN achieves a smaller median deviation compared to the 3-path PDNN, its convergence time over the entire phase is nearly 30% longer. Therefore, we adopt the 3-path PDNN as the implementation algorithm for quadratic programming.

To further optimize the computational efficiency of the algorithm, the experiment incorporates sparse matrix optimization and specialized matrix multiplication optimization. The memory usage and tracking time are evaluated accordingly in Table. IV. The results show that these two optimizations dramatically reduce the random access memory (RAM) usage and accelerate the tracking speed of the attitude trajectory, which provides strong support for resource-constrained embedded hardware operation.

**IEEE Robotics and Automation Letters (RA-L) paper, presented at ICRA 2026, Vienna, Austria. Cite as RA-L paper.**

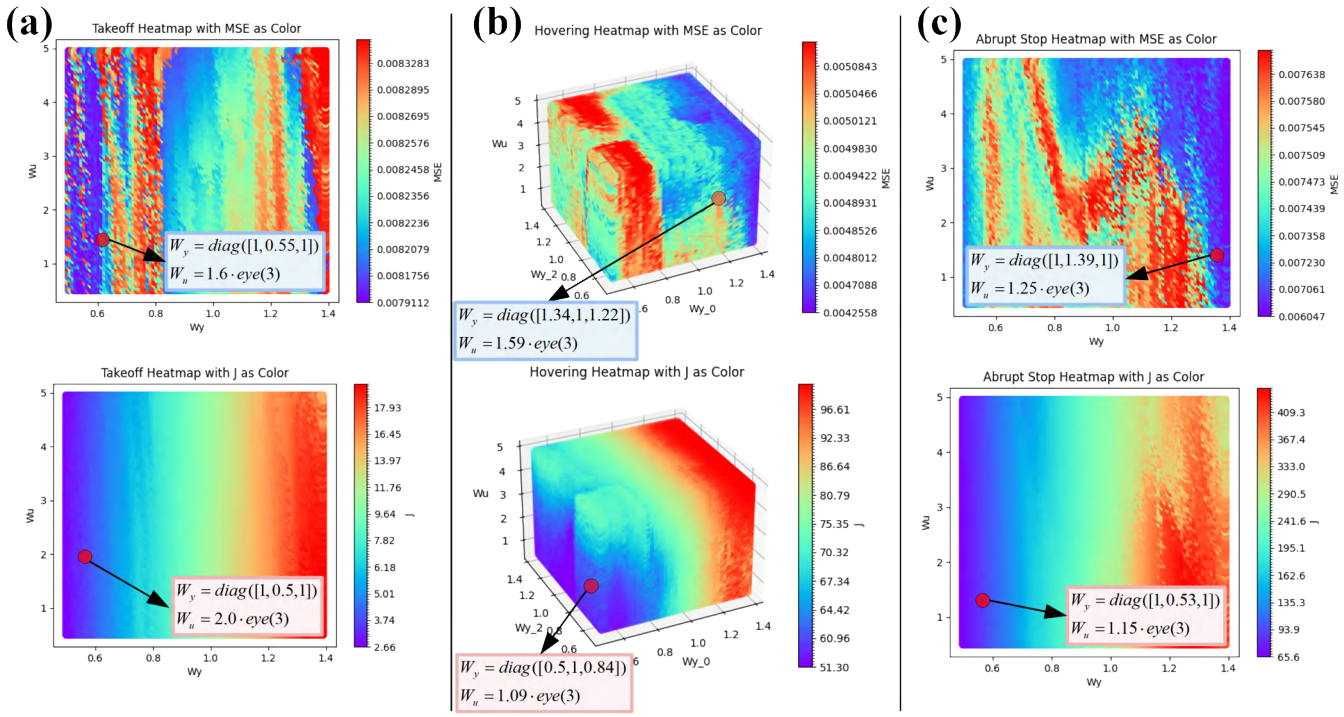


Fig. 5: The heatmap of weight parameters' selection with MSE and with J as the heat value, respectively.

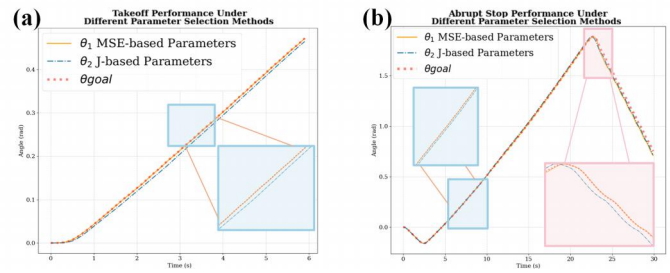


Fig. 6: Performance under different parameter selection methods: (a) Takeoff performance. (b) Abrupt stop performance.

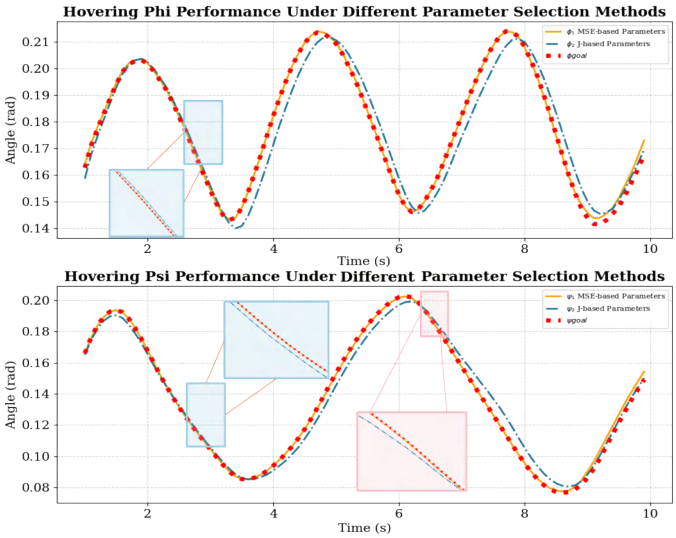


Fig. 7: Hovering performance under different parameter selection methods.

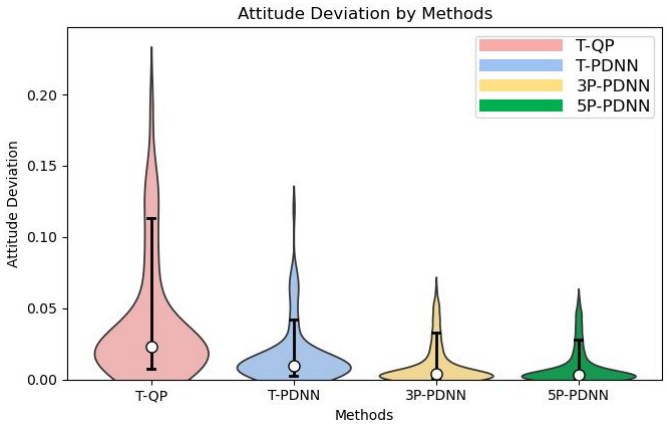


Fig. 8: Attitude deviation by different methods.

Note: In the figure, T-QP represents the traditional quadratic programming algorithm, T-PDNN represents the traditional PDNN algorithm, 3P-PDNN refers to the PDNN algorithm optimized with three-path optimization, and 5P-PDNN refers to the PDNN algorithm optimized with five-path optimization.

### *C. Real-World Deployments of Attitude Tracking*

We conducted a series of hardware experiments. L-BIRD's hardware platform is equipped with the XC7Z100, and the model algorithm runs in standalone mode, enabling high-speed local computation of the controller. This allows real-time attitude estimation and control command generation to be performed on a resource-constrained platform without reliance on an external processor.

Using the weight parameter pair determined from the above conclusions, L-BIRD successfully completed a full flight sequence, including takeoff from a stationary state, stable

IEEE Robotics and Automation Letters (RA-L) paper, presented at ICRA 2026, Vienna, Austria. Cite as RA-L paper.

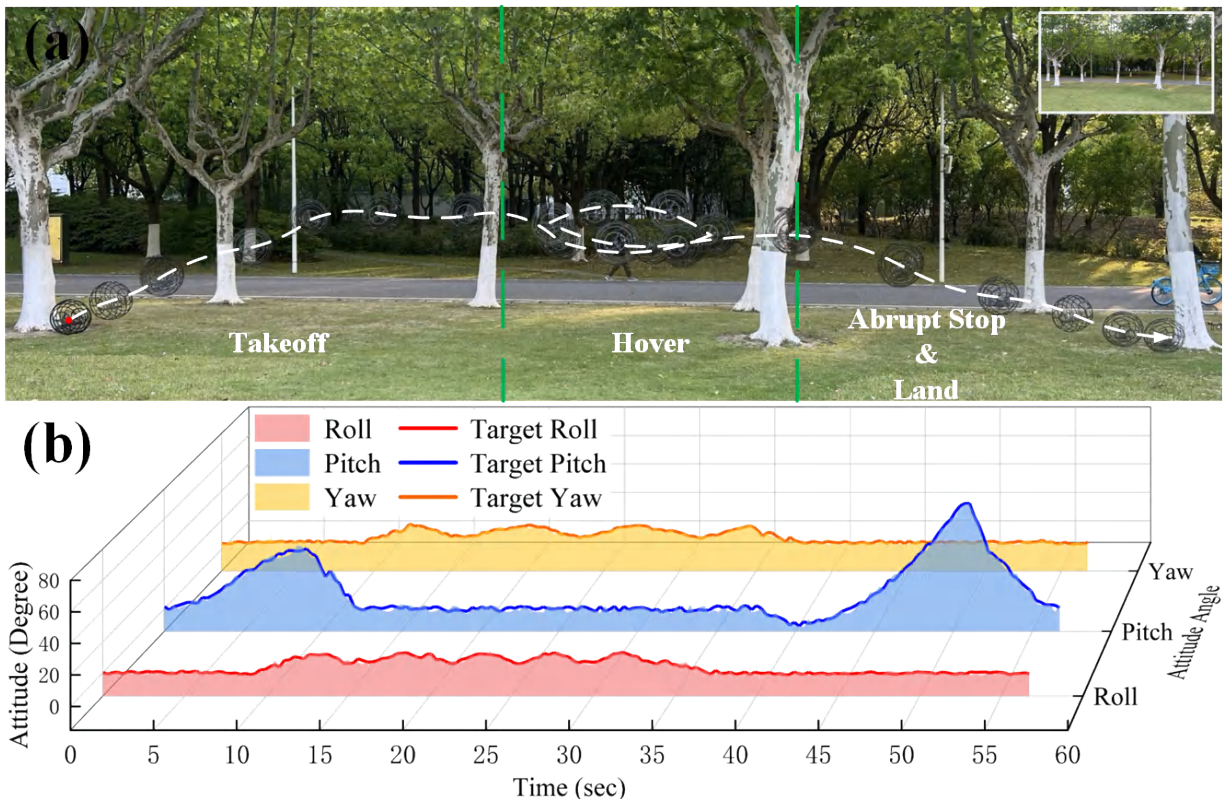


Fig. 9: Flight phases and attitude tracking performance of L-BIRD: (a) The time-lapse image of entire flying task. (b) The comparison of real and target attitude.

TABLE IV
RAM USAGE AND TRACK TIME FOR DIFFERENT MODELS

| | Takeoff | | Hovering | | Abrupt Stop | |
|---|---|---|---|---|---|---|
| | RAM Usage(KB) | Track Time (s) | RAM Usage(KB) | Track Time (s) | RAM Usage(KB) | Track Time (s) |
| **PDNN** | 146.1 | 0.167 | 144.8 | 0.320 | 150.3 | 0.615 |
| **PDNN-S** | 107.4 | 0.128 | 102.2 | 0.280 | 109.8 | 0.486 |
| **PDNN-S-OM** | 89.3 | 0.087 | 88.2 | 0.103 | 90.7 | 0.165 |

Note: In the table, PDNN represents the three-path optimized PDNN model, PDNN-S represents the three-path optimized PDNN model with sparse matrix optimization, and PDNN-S-OM represents the three-path optimized PDNN model with both sparse matrix optimization and specialized matrix multiplication optimization.

hovering, and deceleration into an abrupt stop. During the real-world deployments, we use a camera (FUJIFILM XS20, 100 fps) to capture the position of the robot during three flying phases, the time-lapse images of the entire flying task are shown in Fig. 9(a). We use onboard gyroscopic sensors to collect L-BIRD's attitude angle data during controlled flight. Fig. 9(b) illustrates the variations of all three attitude angles throughout the full flight phase, compared with the target attitude trajectories. The root mean square error (RMSE) between the measured and target attitudes was calculated as $2.8^\circ$ (roll), $3.5^\circ$ (pitch), and $4.1^\circ$ (yaw), confirming that the tracking accuracy remained within $5^\circ$ throughout the task.

### *D. Environmental Adaptability Test*

Fig. 10 shows several usage scenarios of the L-BIRD. In some complex or hazardous ground, such as post-disaster areas, mine caves, etc., the rugged terrain makes landing impossible for normal aircraft. We designed a disturbance experiment (Fig. 10(a)), which demonstrates that L-BIRD can rapidly return to its target attitude trajectory after being

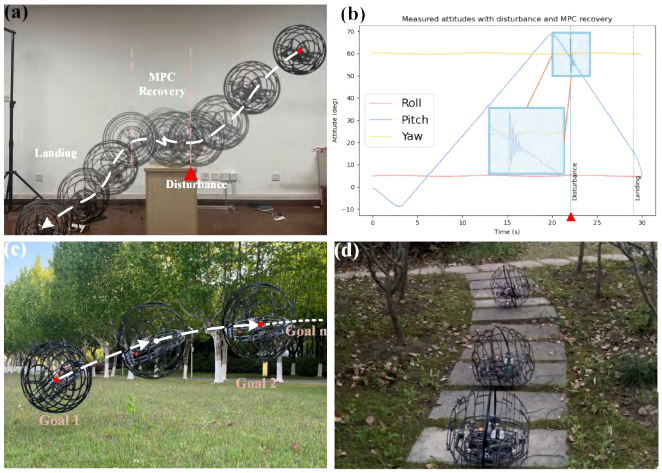


Fig. 10: Environmental adaptability test: (a) Experiment with disturbance. (b) Measured attitudes in the experiment. (c) Fly to next target. (d) Roll through narrow space.

disturbed, with the attitude angle variations shown in Fig. 10(b). This performance is attributed to the MPC algorithm's capability for predictive and constraint-aware control, while the spherical outer shell relaxes the attitude constraints in the QP formulation, thereby reducing the likelihood of constraint violations during landing or disturbance recovery. L-BIRD achieved successful landings within ±35° roll and ±25° pitch, confirming that MPC enables wide-angle surface adaptation beyond structural tolerance. L-BIRD can re-takeoff at any time and fly to the next mission area (Fig. 10(c)). In terrains with narrow takeoff spaces, the spherical structure of the L-BIRD enables rolling movement (Fig. 10(d)), selecting terrains with a wider field of view for further operations.

## V. Conclusions

In this letter, we demonstrate the design of a lightweight bio-inspired rotary-wing drone. L-BIRD is capable of taking off, hovering, abrupt stop and perching like a bird. We constructed a dynamics model of L-BIRD, using the fitted bird attitude as the target attitude trajectory. We improve MPC framework by multi-path PDNN. For lightweight control, we introduce matrix sparsity and multiplicative optimization. The MSE of trajectory tracking averaged over multiple flight phases is only 0.0042 rad in the simulation deployments. Compared to the baseline without optimization strategies, we reduce the RAM usage by 39.3% on average and keep the tracking time of a single step within about 5.17 ms. In real-world flight deployments, our L-BIRD holds environmental adaptability. It can takeoff and land flexibly on complex surfaces, perform low-power perching, and roll in narrow space. It holds substantial potential for complex tasks such as wildlife monitoring and mine tunnel inspection. Future efforts will concentrate on imitating a wider range of bird behaviors, such as predation and fights, in order to more effectively replicate birds' agility and responsiveness.

## References


[1] A. Wissa, "Trade-offs between stability and manoeuvrability in bird flight," *Nature*, 2022.

[2] C. Harvey, V. Baliga, J. Wong, D. Altshuler, and D. Inman, "Birds can transition between stable and unstable states via wing morphing," *Nature*, vol. 603, no. 7902, pp. 648–653, 2022.

[3] C. Harvey, L. L. Gamble, C. R. Bolander, D. F. Hunsaker, J. J. Joo, and D. J. Inman, "A review of avian-inspired morphing for uav flight control," *Prog. Aerosp. Sci.*, vol. 132, p. 100825, 2022.

[4] X. Zhang, G. Cheng, and G. Chen, "A new type bionic foldable wing design for high maneuverable unmanned aerial vehicle," *Appl. Sci.*, vol. 13, no. 14, p. 8345, 2023.

[5] A. Sofla, S. Meguid, K. Tan, and W. Yeo, "Shape morphing of aircraft wing: Status and challenges," *Mater. Des.*, vol. 31, no. 3, pp. 1284–1292, 2010.

[6] A. Pantoja and J. E. G. Yela, "Nonlinear control of a quadrotor for attitude stabilization," in *Proc. IEEE Colomb. Conf. Autom. Control (CCAC)*. IEEE, 2017, pp. 1–6.

[7] Q. Han, Z. Liu, H. Su, and X. Liu, "Filter-based adaptive backstepping attitude control for multi-rotor uavs with parametric uncertainty, external disturbance and input saturation," *Nonlinear Dyn.*, vol. 112, no. 20, pp. 18 293–18 310, 2024.

[8] O. Moali, D. Mezghani, A. Mami, A. Oussar, and A. Nemra, "Uav trajectory tracking using proportional-integral-derivative-type-2 fuzzy logic controller with genetic algorithm parameter tuning," *Sensors*, vol. 24, no. 20, p. 6678, 2024.

[9] J. Moreno-Valenzuela, R. Pérez-Alcocer, M. Guerrero-Medina, and A. Dzul, "Nonlinear pid-type controller for quadrotor trajectory tracking," *IEEE/ASME Trans. Mechatron.*, vol. 23, no. 5, pp. 2436–2447, 2018.

[10] M. Z. Anwar, B. W. Tobalske, S. Agrawal, J.-M. Mongeau, H. Luo, and B. Cheng, "Hummingbirds rapidly respond to the removal of visible light and control a sequence of rate-commanded escape manoeuvres in milliseconds," *Proc. R. Soc. B*, vol. 291, no. 2035, p. 20241268, 2024.

[11] G. Xin and M. Mistry, "Optimization-based dynamic motion planning and control for quadruped robots," *Nonlinear Dyn.*, vol. 112, no. 9, pp. 7043–7056, 2024.

[12] M. Schwenzer, M. Ay, T. Bergs, and D. Abel, "Review on model predictive control: An engineering perspective," *Int. J. Adv. Manuf. Technol.*, vol. 117, no. 5, pp. 1327–1349, 2021.

[13] H. F. Vogel, V. E. A. McCarron, and J. J. Zocche, "Use of artificial perches by birds in ecological restoration areas of the cerrado and atlantic forest biomes in brazil," *Neotrop. Biol. Conserv.*, vol. 13, no. 1, p. 24, 2018.

[14] A. Castillo-Escrivà, G. M. López-Iborra, J. Cortina, and J. Tormo, "The use of branch piles to assist in the restoration of degraded semiarid steppes," *Restor. Ecol.*, vol. 27, no. 1, pp. 102–108, 2019.

[15] R. Zufferey, J. Tormo-Barbero, D. Feliu-Talegón, S. R. Nekoo, J. Á. Acosta, and A. Ollero, "How ornithopters can perch autonomously on a branch," *Nat. Commun.*, vol. 13, no. 1, p. 7713, 2022.

[16] W. R. Roderick, M. R. Cutkosky, and D. Lentink, "Bird-inspired dynamic grasping and perching in arboreal environments," *Sci. Robot.*, vol. 6, no. 61, p. eabj7562, 2021.

[17] A. Briod, P. Kornatowski, J.-C. Zufferey, and D. Floreano, "A collision-resilient flying robot," *Journal of Field Robotics*, vol. 31, no. 4, pp. 496–509, 2014.

[18] P. M. Kornatowski, M. Feroskhan, W. J. Stewart, and D. Floreano, "A morphing cargo drone for safe flight in proximity of humans," *IEEE Robotics and Automation Letters*, vol. 5, no. 3, pp. 4233–4240, 2020.

[19] P. Zheng, F. Xiao, P. H. Nguyen, A. Farinha, and M. Kovac, "Metamorphic aerial robot capable of mid-air shape morphing for rapid perching," *Sci. Rep.*, vol. 13, no. 1, p. 1297, 2023.

[20] A. Banazadeh and N. Taymourtash, "Adaptive attitude and position control of an insect-like flapping wing air vehicle," *Nonlinear Dyn.*, vol. 85, pp. 47–66, 2016.

[21] R. Beard, C. Cao, and N. Hovakimyan, "An l1 adaptive pitch controller for miniature air vehicles," in *Proc. AIAA Guid. Navig. Control Conf. Exhibit*, 2006, p. 6777.

[22] I. Gregory, C. Cao, E. Xargay, N. Hovakimyan, and X. Zou, "L1 adaptive control design for nasa airstar flight test vehicle," in *Proc. AIAA Guid. Navig. Control Conf.*, 2009, p. 5738.

[23] S. Mallikarjunan, B. Nesbitt, E. Kharisov, E. Xargay, N. Hovakimyan, and C. Cao, "L1 adaptive controller for attitude control of multirotors," in *Proc. AIAA Guid. Navig. Control Conf.*, 2012, p. 4831.

[24] H. Nguyen, M. Kamel, K. Alexis, and R. Siegwart, "Model predictive control for micro aerial vehicles: A survey," in *Proc. Eur. Control Conf. (ECC)*. IEEE, 2021, pp. 1556–1563.

[25] M. Kamel, M. Burri, and R. Siegwart, "Linear vs nonlinear mpc for trajectory tracking applied to rotary wing micro aerial vehicles," *IFAC-Pap. Online*, vol. 50, no. 1, pp. 3463–3469, 2017.

[26] M. Bangura and R. Mahony, "Real-time model predictive control for quadrotors," *IFAC Proc. Vol.*, vol. 47, no. 3, pp. 11 773–11 780, 2014.

[27] D. Shi, J. Yin, and C. Bai, "An effective global optimization algorithm for quadratic programs with quadratic constraints," *Symmetry*, vol. 11, no. 3, p. 424, 2019.

[28] K. Nguyen, S. Schoedel, A. Alavilli, B. Plancher, and Z. Manchester, "Tinympc: Model-predictive control on resource-constrained microcontrollers," in *2024 IEEE International Conference on Robotics and Automation (ICRA)*. IEEE, 2024, pp. 1–7.

[29] T. Nath, A. Mathis, A. C. Chen, A. Patel, M. Bethge, and M. W. Mathis, "Using deeplabcut for 3d markerless pose estimation across species and behaviors," *Nature protocols*, vol. 14, no. 7, pp. 2152–2176, 2019.

[30] J. Hägerlind, J. Hentati-Sundberg, and B. Wandt, "Temporally-consistent 3d reconstruction of birds," *arXiv preprint arXiv:2408.13629*, 2024.

[31] Y. Zhang, "On the lvi-based primal-dual neural network for solving online linear and quadratic programming problems," in *Proceedings of the 2005, American Control Conference, 2005.* IEEE, 2005, pp. 1351–1356.

[32] Y. Zhang, W. Ma, X.-D. Li, H.-Z. Tan, and K. Chen, "Matlab simulink modeling and simulation of lvi-based primal–dual neural network for solving linear and quadratic programs," *Neurocomputing*, vol. 72, no. 7-9, pp. 1679–1687, 2009.